Turk J Engin Environ Sci
24 (2000) , 383 – 399.

Modeling and Parameter Identification of a Pneumatic Constant Force Device

Levent GÜVENÇ
İstanbul Technical University, Department of Mechanical Engineering,
Gümüşsuyu, Taksim, İstanbul-TURKEY
Krishnaswamy SRINIVASAN
The Ohio State University, Department of Mechanical Engineering,
Columbus, Ohio, USA

Received 02.02.1999

Abstract

Robot-assisted material removal applications necessitate the use of active end effectors under force or compliance control for satisfactory performance. Constant force devices with pneumatic actuators, even though nonprogrammable, are the cheapest and least complicated active end effectors that are available and are expected to be useful in applications where wide changes in operating conditions are not encountered. The pneumatic circuit of such a constant force device is modeled in this paper as a prerequisite to its evaluation for robot-assisted material removal. Pneumatic model parameters are identified experimentally using an iterative maximum likelihood search. The method used here for modeling and numerical model parameter determination is general in nature and can be applied to other pneumatic systems after some modifications.

Key Words: pneumatic modeling, experimental model parameter determination, constant force devices

Pnömatik Bir Sabit Kuvvet Cihazının Modellenmesi ve Model Parametrelerinin Tanınması

Özet

Robot destekli talaş kaldırma uygulamalarında istenilen performansa ulaşmak için kuvvet ya da esneklik denetimi altında çalışan aktif tutucular kullanılır. Pnömatik tahrik elemanları içeren sabit kuvvet cihazları, programlanabilir olmamalarına rağmen bu tip aktif tutucuların arasında en ucuz ve basit olanlarıdırlar ve çalışma koşullarının çok büyük değişiklikler göstermediği uygulamalarda kullanılırlar. Bu makalede robot destekli talaş kaldırma işlemlerinde kullanım uygunluğunun tesbiti için böyle bir sabit kuvvet cihazının pnömatik devresi modellenmiş ve model parametrelerinin sayısal değerleri iteratif bir maksimum olasılık tarama algoritması kullanılarak deneysel olarak belirlenmiştir. Burada kullanılan modelleme ve parametre tanıma yöntemi genel karakterde olup ufak değişikliklerle başka pnömatik sistemlere de uygulanabilir.

Anahtar Sözcükler: pnömatik sistem modellenmesi, model parametrelerinin deneysel olarak belirlenmesi, sabit kuvvet cihazları

1. Introduction

Constant force devices are used to regulate tool-workpiece contact force in robot-assisted material removal tasks. In pneumatically powered constant force devices, control of the contact force is achieved indirectly by regulation of pressure in the actuating air cylinder. The presence of a pressure regulator results in a high gain feedback loop for maintaining constant cylinder pressure. This control arrangement is also called load control. As is true for any control system, a good model of the system's dynamic elements, which are mainly the regulator and the cylinder here, is needed to evaluate performance and for design purposes. The pneumatic components of a commercially available constant force device, referred to hereafter as CFD2100, are modeled here. The CFD2100 was designed to provide real-time control of applied tooling force in robotic deburring and surface conditioning applications (Alvite and Gearman, 1988). There are two opposing low friction air cylinders coupled with high resolution pressure regulators in this device. The difference in the constant pressures in the two cylinders, multiplied by the piston cross-sectional area and a geometric factor, results in the static applied load (Güvenç, 1999). The desired force level is set by adjusting the pressure regulators. The CFD2100 is designed as an active end effector for industrial robots; however, it can also be used as a bench-mounted device if the robot holds and manipulates the part. Graf has used this device successfully in robot-assisted deburring of inner holes on a jet engine casing using compliant finishing wheels (Graf, 1988). Similar pneumatic constant force devices that use pressure regulator control of a cylinder have been used successfully as active end effectors in robot-assisted surface finishing applications (Weule and Timmermann, 1990; Brevick and Hanrath, 1992).

The use of active end effectors in robot-assisted material removal processes like deburring and finishing is necessitated by the improved dynamic response made possible by these devices (Güvenç and Srinivasan, 1995). Constant force devices fall under the classification of nonprogrammable active end effectors since their controller is fixed by hardware and cannot be changed through programming. Hence, their adaptability to changes in controller design requirements, arising from changes in operating conditions of the material removal process, is limited. Wide changes in the operating conditions necessitate the use of a programmable active end effector, which is much more expensive since it has a separate sensor and associated signal conditioning circuitry to measure the interaction force directly, and a separate microcomputer for control. Thus, the low cost associated with a constant force device motivates its use in robot-assisted material removal tasks when a limited range of changes in the operating conditions is encountered.

An accurate model of the dynamics of a constant force device is needed for determination of the limited range of operating conditions mentioned above, and its performance in robot-assisted material removal applications. Motivated by this need for model development, the pneumatic circuitry of the CFD2100 is analyzed and modeled in this paper using lumped parameter analysis and small signal linearization. More detailed information about the mechanical model of the CFD2100 and its use in robot-assisted material removal can be found in Güvenç (1999).

The approach taken here is general in nature, making it applicable to other instances of a pneumatic cylinder controlled by a pressure regulator, after slight modifications. The available maximum likelihood estimation routine in a commercially available control system analysis, design and simulation software package is used to determine pneumatic model parameters by minimizing the output error between experimental and simulated responses to step-like piston displacement inputs, the tests being conducted on an isolated cylinder and pressure regulator pair of the CFD2100. Although the modeling work reported in this paper is applied to the pneumatic components of the CFD2100, another aim of this paper is to present a general method for determining an accurate model of a pressure-regulated pneumatic cylinder subject to external piston position inputs.

2. Pneumatic Model Development

The pneumatic circuit for a cylinder-regulator combination is shown schematically in Figure 1. The filter traps moisture in the incoming air, and the precision pneumatic pressure regulator, with a maximum flow capacity of 40 scfm, exhaust capacity of 5.5 scfm (downstream pressure 5 psig above set pressure), and a sensitivity of 0.0045 psig, regulates the cylinder pressure. Each single-acting cylinder has a glass body for low friction, and ball and socket joints

on the piston connecting rod to ensure linear piston motion.

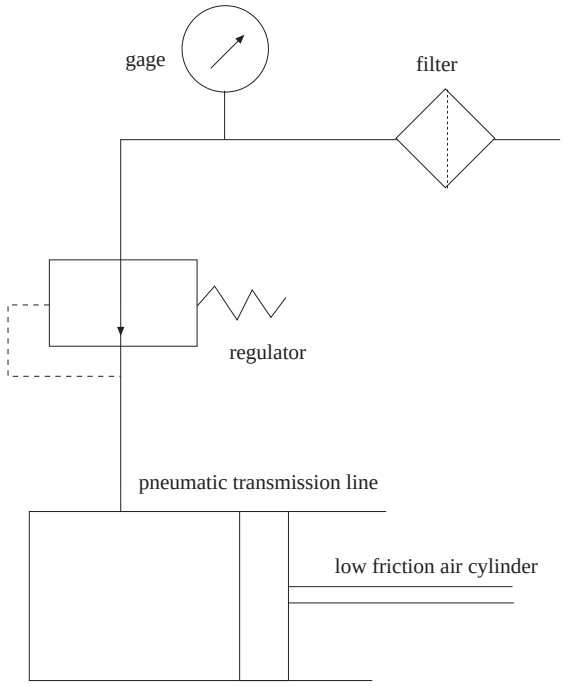

Figure 1. CFD2100 Pneumatic Circuit

When the regulator is adjusted for a specific set point, the downward force of the positive bias spring causes the diaphragm assembly to move downward, opening the supply valve and allowing air to be routed to the outlet port (see Figure 2). At equilibrium, the downward force exerted by the positive bias spring balances the upward force exerted by the downstream pressure, communicated through the aspirator tube on the bottom of the control diaphragm.

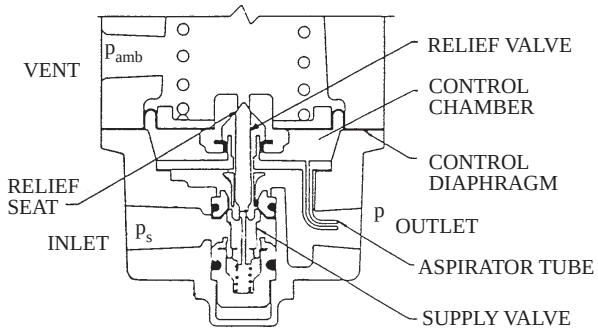

Figure 2. Pressure Regulator

If downstream pressure decreases below a set point, the decrease in pressure, transmitted through the aspirator tube, causes the control diaphragm assembly to move downward, lowering the relief seat against the relief valve, opening the supply valve and allowing downstream pressure to rise until a set point value is reached. This process where the flow from the inlet (supply) to the outlet takes place is called charging. The mass flow rate dM_c/dt for charging is given by

$$\frac{dM_c}{dt} = 0.449\frac{p_s}{\sqrt{T_s}}\left(1 + 0.537\frac{p}{p_s}\right)\left(1 - \frac{p}{p_s}\right)^{1/2} A_{s\nu} \tag{1}$$

where p_s, T_s, p and A_{sv} are the absolute supply pressure and temperature, absolute outlet pressure, and effective supply to outlet orifice area respectively, and sonic flow with $p/p_s < 0.528$ has been assumed (Andersen, 1976). The constant term in Equation (1) depends on the unit system used (British system here) but the results are not affected by its numerical value. The supply pressure p_s is in the range of 70 to 80 psig here and the outlet pressure p for the CFD2100 cylinders, both cylinders being under pressure regulator control, is limited to 30 psig, thus justifying the sonic flow assumption used. Assuming the supply pressure and temperature to be constant and assuming small percent changes in p/p_s, (1) can be re-expressed as

$$\frac{dM_c}{dt} = K_2 A_{s\nu} \tag{2}$$

by lumping the expression multiplying A_{sv} into one term, K_2, which becomes a constant after linearization about the operating region. Note that the linearized model in (2) would still be obtained if a subsonic flow relation had been used instead of the sonic flow relation of (1). The numerical values of K_2 in (2) will vary, however, depending on whether the flow conditions are sonic or subsonic.

If the downstream pressure rises above the set point, the increase in pressure, transmitted through the aspirator tube, acts on the bottom of the control diaphragm assembly, moving it upward to allow supply valve seating. As the diaphragm assembly slides upward, the relief seat moves away from the relief valve and air is exhausted through the vent. The exhausting process, with flow from the outlet to the vent, is called discharging. The flow rate dM_d/dt for discharging is governed by a relation similar to (1), except that the ambient pressure, p_{amb}, and p replace p and p_s respectively in (1), if the flow is sonic

with $p_{amb}/p < 0.528$. Again, assuming constant supply pressure and temperature and small changes in p_{amb}/p,

$$\frac{dM_d}{dt} = -K_3 A_\nu \tag{3}$$

where K_3 is a constant obtained after linearization, and A_v is the effective outlet to vent orifice area. The sonic flow assumption may not be justified for low outlet pressures p, however, and a subsonic mass flow rate equation, which will still result in the linearized model form of (3), but with a different numerical value for K_3, must be used.

The dynamic relation between the outlet pressure p and control chamber pressure p_f is developed next. The flow from the outlet to the control chamber through the aspirator tube is modeled as laminar flow through a circular tube (Andersen, 1976), and is given by

$$\frac{dM_a}{dt} = \rho_{a\nu} \frac{D^2}{32\mu} \frac{A}{L} (p - p_f) \tag{4}$$

where $dM_a/dt, \rho_{av}, D, \mu, L$ and A are the mass rate of flow through the aspirator tube, the average of upstream and downstream densities, the inner diameter of the aspirator tube, the viscosity of air, the length of the aspirator tube and the cross-sectional area of the aspirator tube, respectively. Equation (4) can also be expressed as

$$\frac{dM_a}{dt} = K_1 (p - p_f) \tag{5}$$

where K_1 is constant for constant air density and viscosity. Assuming a polytropic charging process inside the control chamber, the change in chamber pressure is governed by

$$\frac{dp_f}{dt} = \frac{np_f}{M_a} \frac{dM_a}{dt} \tag{6}$$

where n and M_a are the polytropic constant for air and the mass of air entrapped inside the control chamber, respectively (Andersen, 1976). (5) and (6) can be combined to obtain

$$\frac{dp_f}{dt} = \frac{np_f}{M_a} K_1 (p - p_f) \tag{7}$$

which is a nonlinear differential equation relating the difference between the outlet and control chamber pressures to the control chamber or sensed pressure. (7) will be linearized assuming an almost constant M_a and small changes in p_f around an operating region. The linearization, further algebraic manipulations and application of the Laplace transform on equation (7) result in

$$p_f = \frac{p}{\tau s + 1} \tag{8}$$

where $\tau \equiv \frac{\overline{M}_a}{n \overline{p}_f K_1}$ and the overbars have been used to denote equilibrium values appropriate for the operating region.

Calculation of the effective charging and discharging areas A_{sv} and A_v involves modeling the dynamics of the mass-spring systems associated with the supply and relief valve mechanisms. These effective area changes are simply modeled by

$$A_{sv} = K_4 (p_d - p_f) \tag{9}$$

$$A_v = K_5 (p_f - p_d) \tag{10}$$

assuming that the area changes occur at frequencies that lie well within the bandwidths of the mechanical systems responsible for supply and relief valve operation. This assumption is justified as the stiffness to moving mass ratio of the pressure regulating valve is very high. K_4 and K_5 are constants and p_d is the desired pressure, proportional to the set spring force. The pneumatic transmission line dynamics are assumed to be negligible for the short lines connecting the pressure regulators to the cylinders in the CFD2100. Thus, the cylinder pressures are assumed to be the same as the corresponding regulator output pressures.

For a bench-mounted CFD2100, the cylinder base is fixed (see Figure 3) and forms an inertial frame of reference, with x_c representing the piston displacement relative to it. If $p < p_f$, there will be flow from the supply to the outlet through the supply valve, charging the cylinder according to

$$\frac{dp_c}{dt} = \frac{np_c}{M_c} \frac{dM_c}{dt} - \frac{np_c}{V_c} A_c \dot{x}_c \tag{11}$$

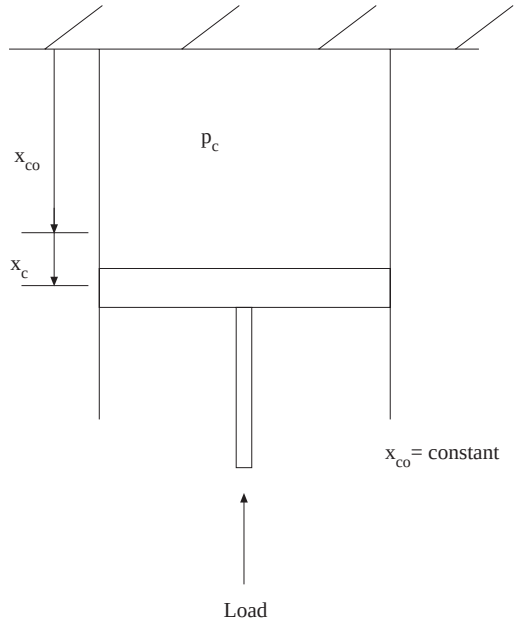

Figure 3. The Cylinder

where M_c and A_c are the mass of air inside and the cross-sectional area of the cylinder, respectively (Andersen, 1976). The cylinder discharging flow rate equation will be similar to (11) except for a replacement of dM_c/dt for the charging case with dM_d/dt for discharging. The cylinder pressure p_c is assumed to be the same as the outlet pressure p here and will be replaced by it from now on.

Substituting from (2) and (9) for charging, or (3) and (10) for discharging, into (11) and using further algebraic manipulations, we get

$$\frac{dp_c}{dt} = K(p_d - p_f) - K_x \dot{x}_c \tag{12}$$

where $K = \begin{cases} K_{sv} \equiv K_2 K_4 n p_c / M_c, & p_d < p_f \\ K_v \equiv K_3 K_5 n p_c / M_c, & p_d > p_f \end{cases}$ and $K_x = n p_c A_c / V_c$. Integration of both sides, substitution of p for p_c and use of the Laplace transform variable s in (12) yields

$$p = \frac{K}{s}(p_d - p_f) - K_x x_c \tag{13}$$

Equations (8) and (13) form the basis of the pneumatic model used here and are shown in block diagram form in Figure 4. The switch which chooses the charging or discharging path, with a consequent change in the flow coefficient from K_v to K_{sv} or vice versa, is the only nonlinearity in this model, all other nonlinearities having been simplified using small signal linearization.

3. Pneumatic Model Parameter Identification

The parameters K_v, K_{sv}, K_x and τ in the pneumatic model for the regulator-cylinder combination of the CFD2100 are identified here by comparing experimental step-like displacement results with simulated ones. The setup used for experiments is shown schematically in Figure 5. The regulated pressure is sensed using a diaphragm-type pressure transducer and the displacement is measured using a linear potentiometer. The pressure transducer and potentiometer are found experimentally to generate output voltages proportional to the input pressure and displacement, respectively. The sensitivities are determined to be 5 V per 25 psig for the pressure transducer, and 3.1736 V/in for the linear potentiometer.

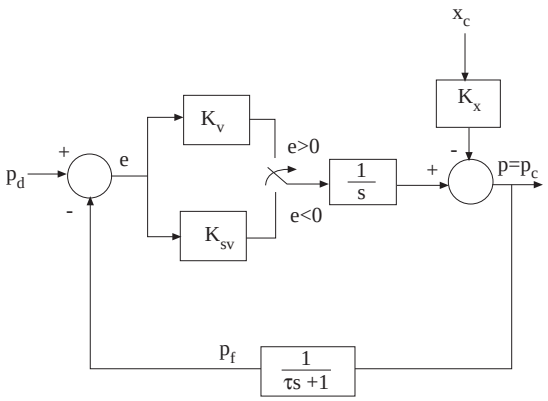

Figure 4. Pneumatic Model

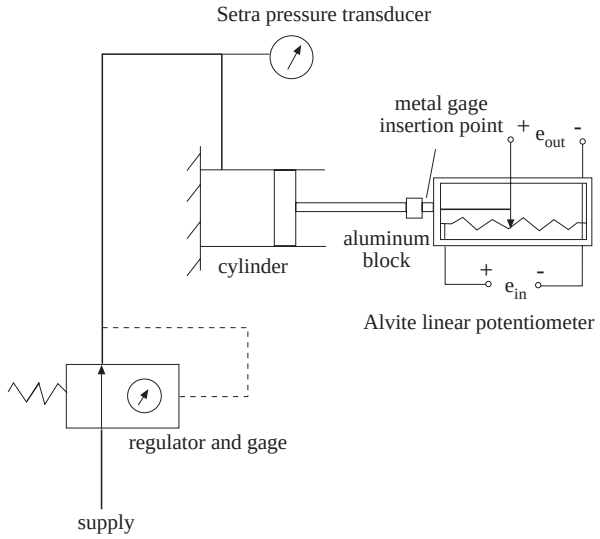

Figure 5. Experimental Setup for Model Determination

The piston is subjected to step-like displacements during the tests by abruptly pulling a metal gage of known thickness, previously inserted between a round aluminum block attached to the piston connecting rod and the linear potentiometer, thus letting the piston travel until the aluminum block hits the potentiometer housing (Figure 5). The piston motion in nonprogrammable active end effectors like the CFD2100 is an external disturbance to the system caused by workpiece surface irregularities and robot tracking errors. The input x_c in the experiments here is therefore used to mimick a step-like workpiece surface irregularity or robot tracking error component. The term step-like instead of step input is used here as the finite time associated with removing the gage block and the neglected inertia of the piston cause the actual input to deviate from the ideal step input. This is not a very critical limitation, however, since the measured disturbance input x_c to the system is used in the numerical parameter determination study.

Pressure and displacement are measured during the test by an Intel 86/310 microcomputer running a data acquisition program written in FORTRAN that triggers from the displacement input and records displacement and pressure data exactly 50 points before and 300 points after the trigger. The lowest possible sampling time of 2 msec is used in data acquisition.

First, step response tests with a position step input of approximately 60 mils, carried out at nominal cylinder pressures of 5, 10, 15 and 20 psig are discussed. Experimental test results are displayed in Figures 6a, 6b through 11a, 11b. As the piston moves forward increasing the volume of air inside the cylinder, the cylinder pressure drops. The pressure regulator then starts to charge air into the cylinder until the pressure reaches the set point and overshoots by a small amount. Set point pressure is reached finally as the excess air is vented through a discharging process.

Some observations based on these experimental results are given below. The pressure responses are, except for small differences, repeatable under the same operating conditions and piston displacement levels as comparisons of Figures 6b and 7b for 5 psig and Figures 8b and 9b for 10 psig of nominal cylinder pressure reveal. The small differences in the responses at the same nominal pressure and the associated differences in the identified parameter values in Table 1 of up to an order of 10% are quite acceptable considering the manual method of supplying the step disturbance input to the system, the slight variations of supply pressure and temperature and the simplifications used in modeling. These observations are true at nominal cylinder pressures of 15 psig and 20 psig as well, although repeated experimental results are not shown here for the sake of brevity. It is also seen that the piston displacement achievable in practice is not exactly a step but more like a fast ramp until the mechanical stop is hit. The delay in observed piston displacement is due to the neglected dynamics of the piston. This is not critical, however, as the measured piston displacement and not an ideal step was used in identification. The actual process of hitting the mechanical stop causes impact forces which result in very high frequency and low amplitude piston oscillations. These piston oscillations are not seen in the displacement plots as the 2 msec sampling interval is not low enough to capture them fully. It is speculated that the high frequency, low amplitude pressure glitches seen in the experimental results are partially due to these piston oscillations and pneumatic transmission line resonances, neglected in the model.

A simulation block diagram of the pneumatic model in Figure 4 was constructed using the SYSTEM_BUILD® block diagram based simulation environment of the control system analysis and design software package MATRIX$_x$®. Experimental piston displacement and cylinder pressure data were transferred to this environment. The simulation model was subject to the constant pressure setpoint input p_d and the experimentally determined piston displacement x_c. The simulated cylinder pressure was compared with the experimentally determined cylinder pressure p_c. The best fit criterion of output error minimization, which in this case is the difference between the simulated and actual pressures, was used in the maximum likelihood search method in MATRIX$_x$® to iteratively change the pneumatic model parameters until a good fit is obtained. Note that other output error based parameter estimation methods could also have been used for numerical parameter value determination. The iterative maximum likelihood search method was preferred as it was readily available and easy to use in the version of MATRIX$_x$® used here.

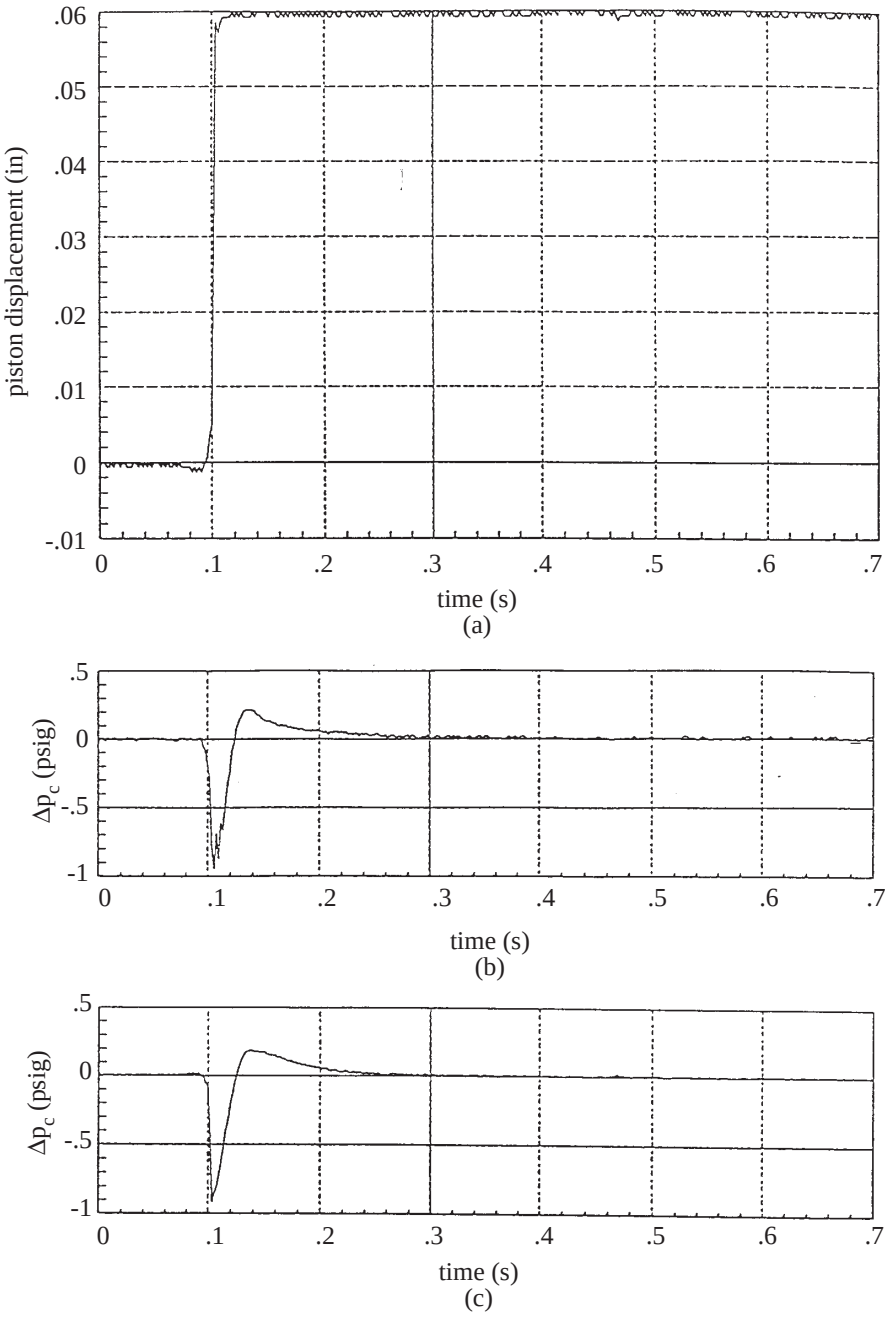

Figure 6. Cylinder Position Step Input (Large) Test for p_c=5 psig. First Time: a) Position Input. b) Change in Pressure. c) Simulated Change in Pressure

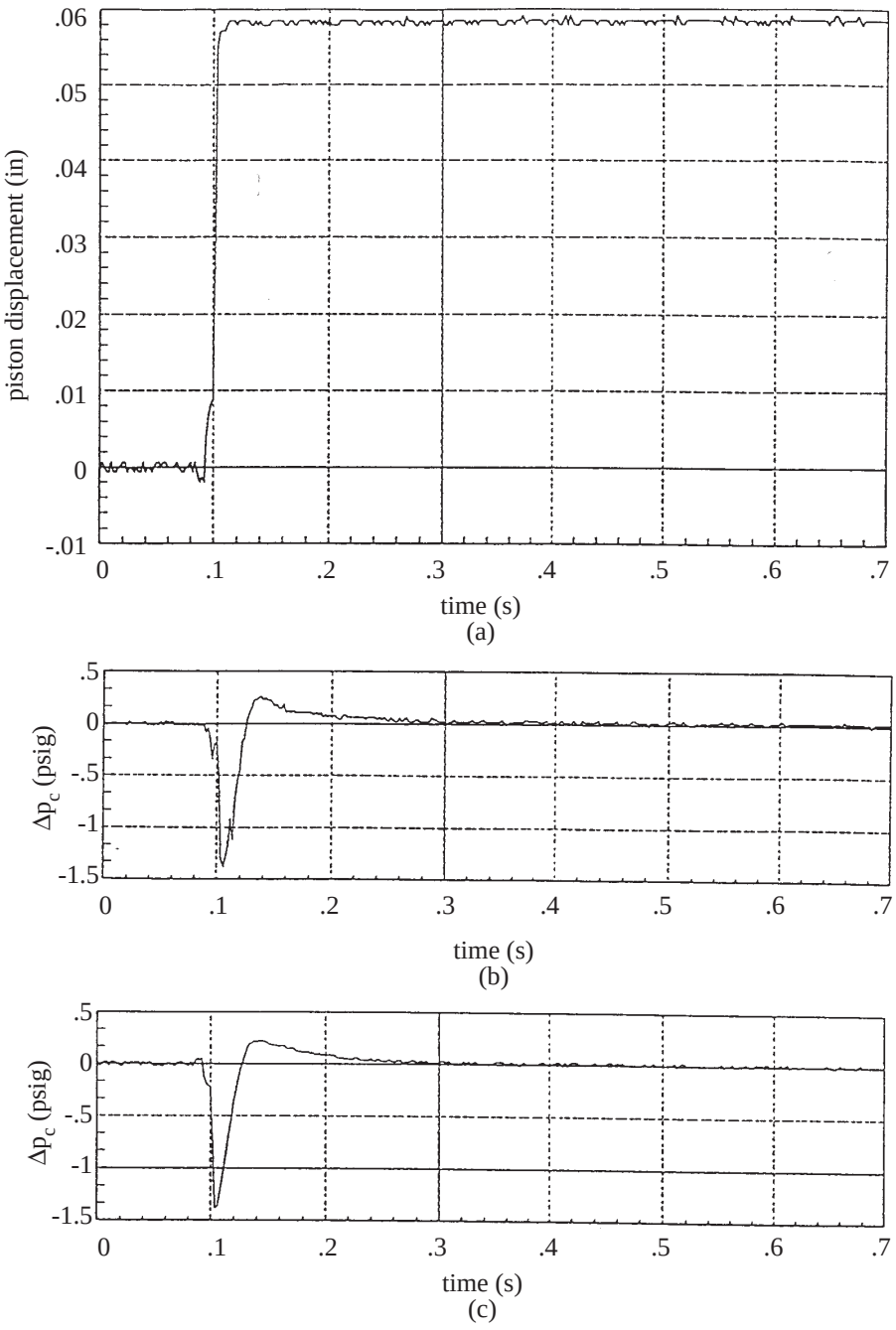

Figure 7. Cylinder Position Step Input (Large) Test for p_c=5 psig. Second Time: a) Position Input. b) Change in Pressure. c) Simulated Change in Pressure

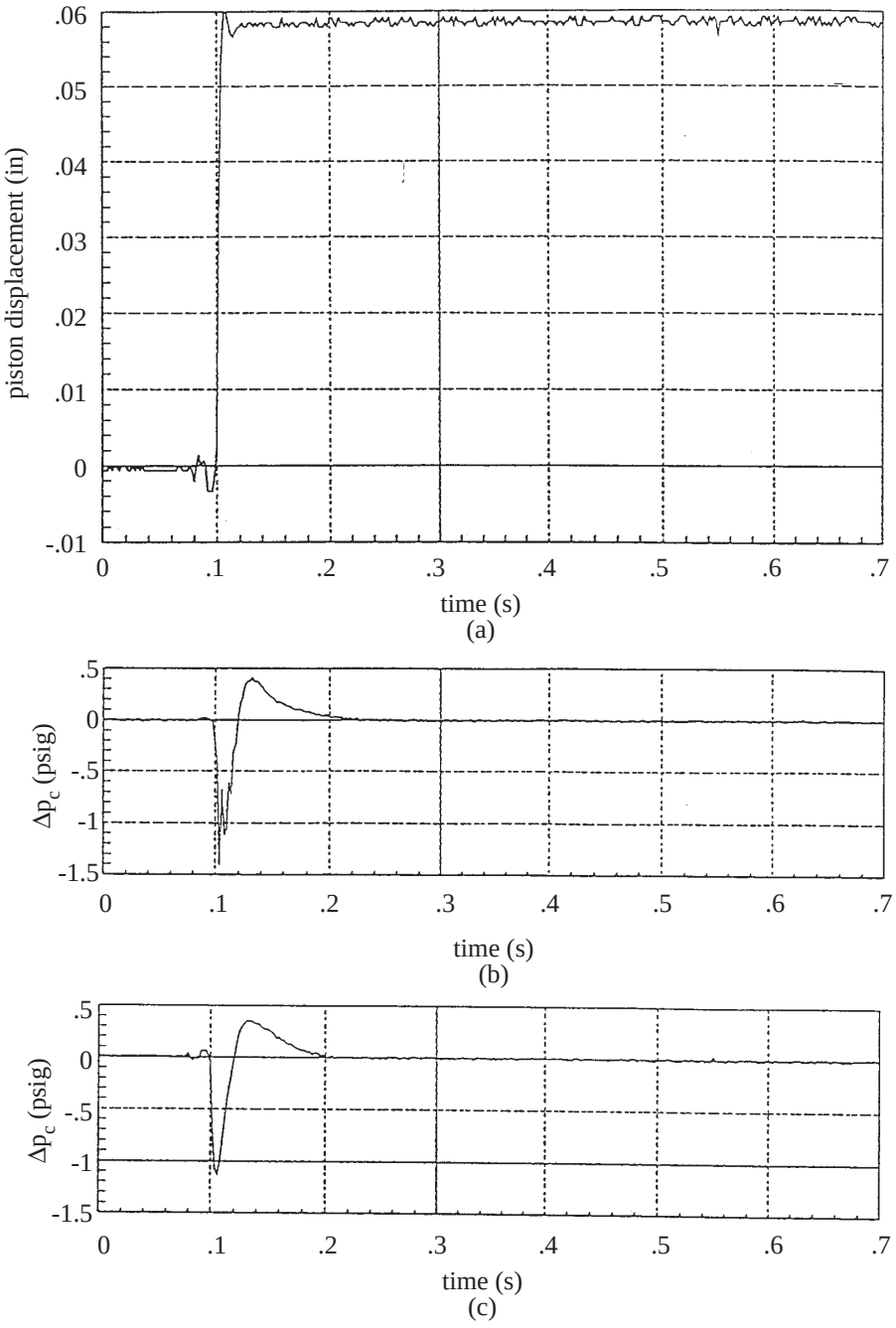

Figure 8. Cylinder Position Step Input (Large) Test for p_c=10 psig. First Time: a) Position Input. b) Change in Pressure. c) Simulated Change in Pressure

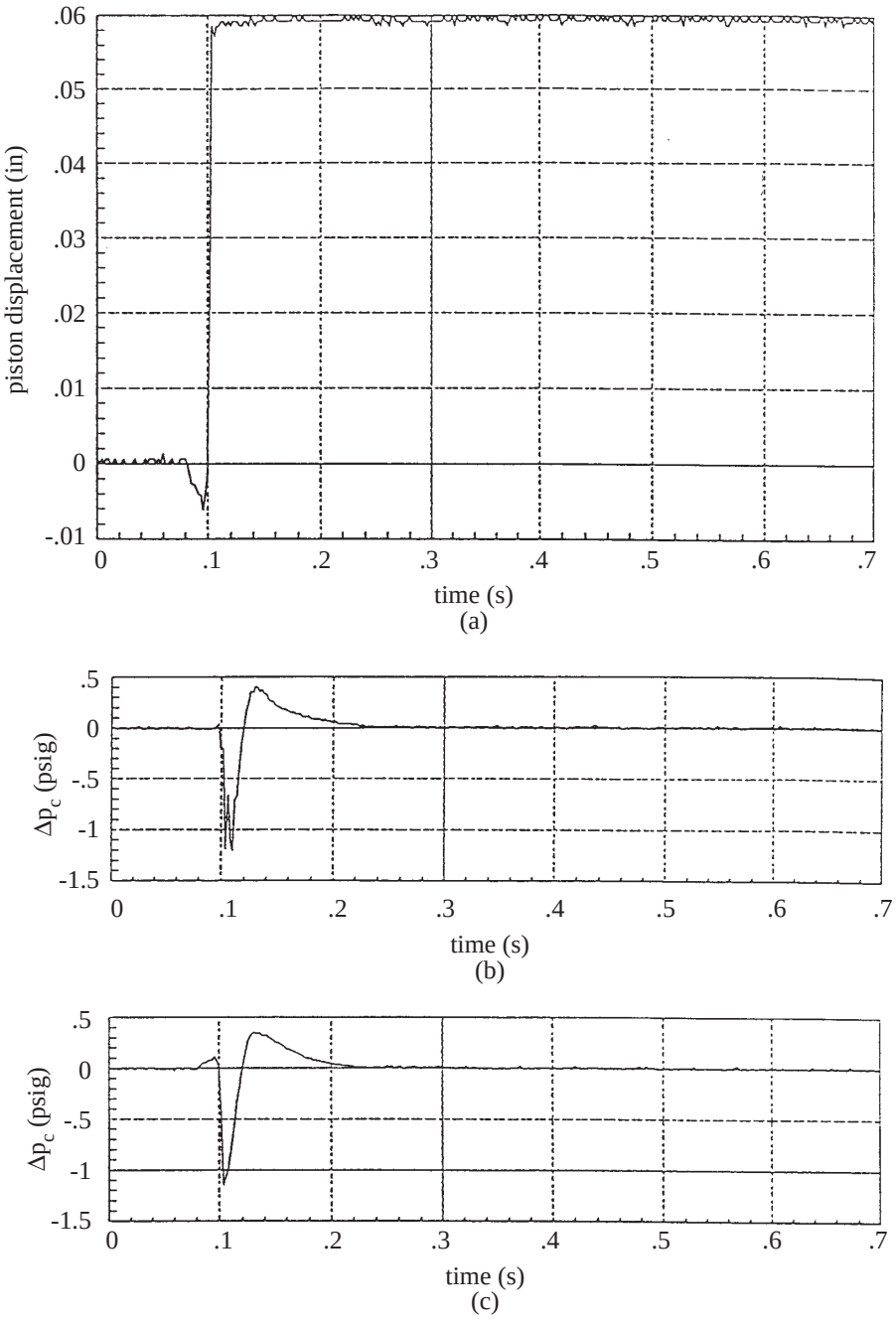

Figure 9. Cylinder Position Step Input (Large) Test for p_c=10 psig. Second Time: a) Position Input. b) Change in Pressure. c) Simulated Change in Pressure

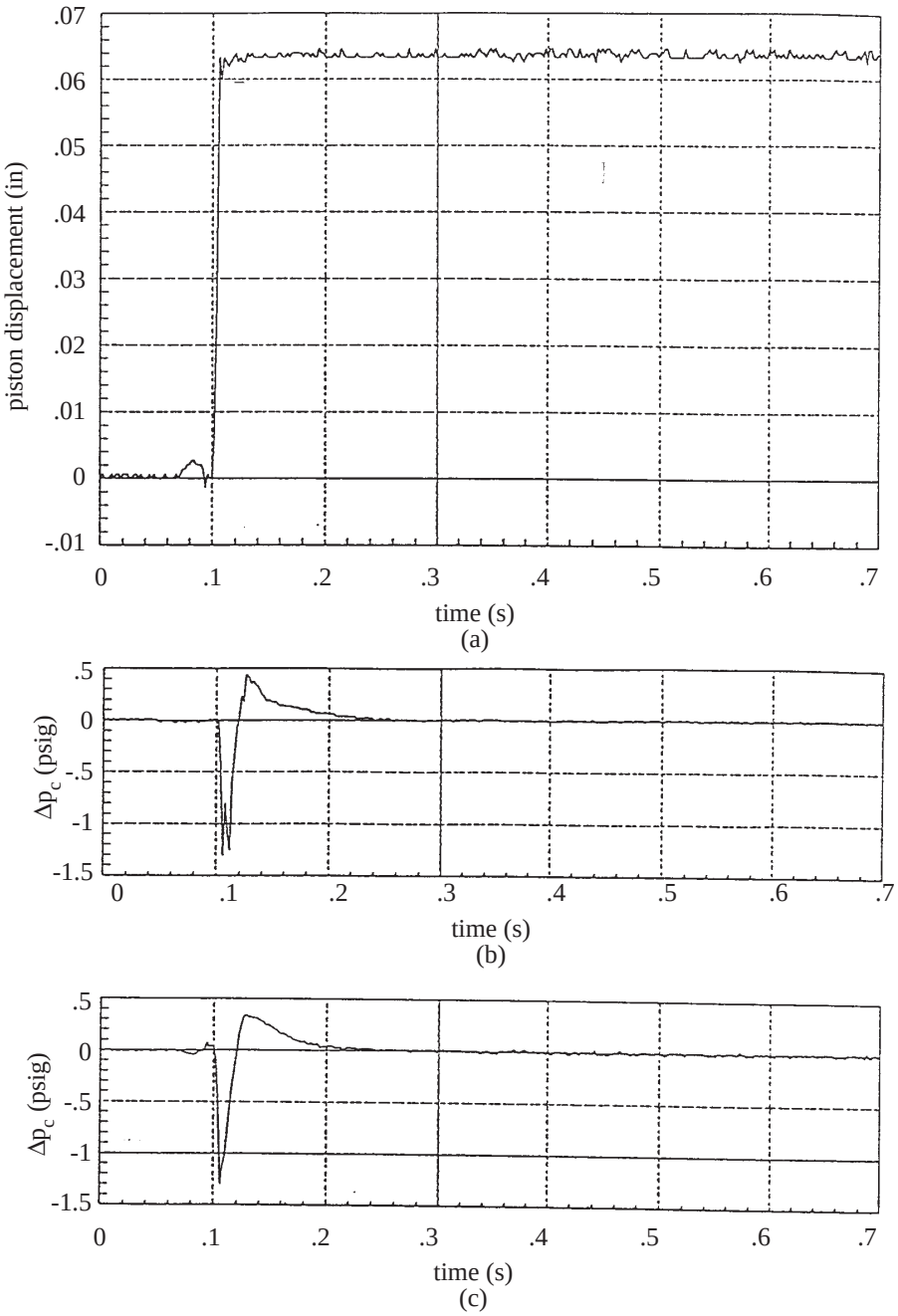

Figure 10. Cylinder Position Step Input (Large) Test for p_c=15 psig: a) Position Input. b) Change in Pressure. c) Simulated Change in Pressure

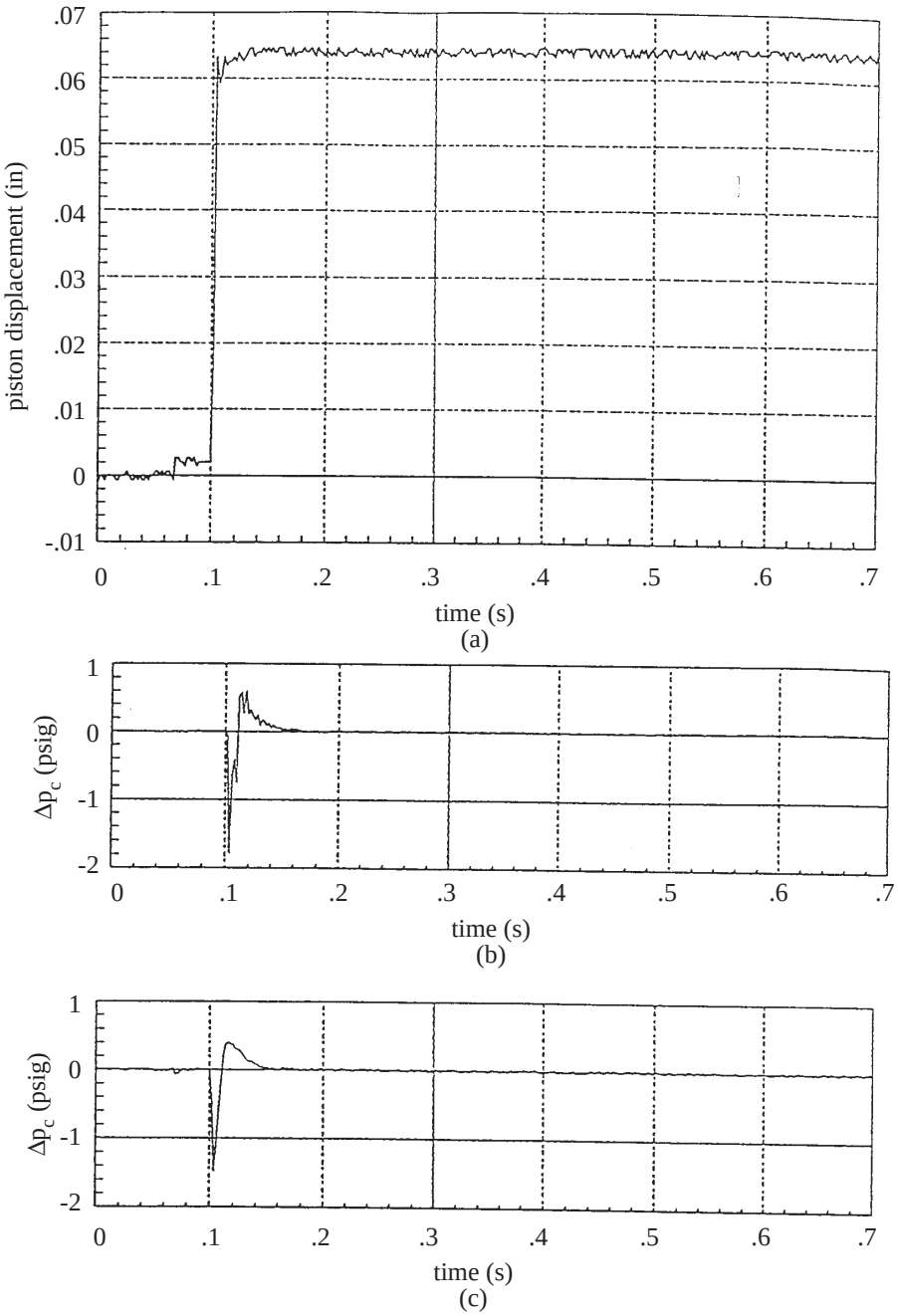

Figure 11. Cylinder Position Step Input (Large) Test for p_c=20 psig: a) Position Input. b) Change in Pressure. c) Simulated Change in Pressure

Table 1. Identified Pneumatic Model Parameters - Large Step

nominal pressure (psig)	K_x (lbf/in^3)	K_{sv} (s^{-1})	K_v (s^{-1})	τ (s)
5	16.0149	112.3780	20.7603	0.0113
5	15.8753	96.2677	18.0990	0.0098
10	20.5522	160.8374	33.5129	0.0126
10	19.6864	168.2485	27.3031	0.0120
15	21.9259	179.918	27.2651	0.0093
20	26.8250	359.8479	57.3027	0.005

The model pressure change responses obtained through this procedure in response to the experimental displacement inputs are displayed in Figures 6c through 11c and are seen to be in good agreement with the experimental results. Identified model parameters are displayed in Table 1 for a range of pressures from 5 to 20 psig. All model parameters except τ are seen to increase in magnitude with increases in nominal cylinder pressure. Extensive simulation studies show that the parameter K_x controls the magnitude of the pressure peak, while the charging and discharging coefficients K_{sv} and K_v control the time it takes the pressure peak to settle down to the set point value. The time constant τ is of the order of 0.01 s for all of the tests. This means that the regulator's pressure sensing dynamic response is faster than the cylinder pressure dynamic response that is being measured. Decreasing τ to values below 0.01 s will not result in any significant change in the simulated pressure, while increasing it will result in pressure oscillations. The effect of model parameter variations on simulated pressure have been summarized graphically in Figure 12.

The discharging coefficient K_v is observed to be smaller than the charging coefficient K_{sv} in the tests (see Table 1). This observation requires an explanation. The experiments that are performed are mainly charging experiments as the piston moves primarily under conditions of increasing cylinder pressure with the setup used here. Any discharging process is due to an overshoot of cylinder pressure during pressure regulation, a common phenomenon in high gain feedback control systems. If piston motions of the same magnitude but in the opposite direction (decreasing cylinder volume) could be produced with the test setup used, different discharging coefficients K_v would probably be obtained given the nonlinear system characteristics. The magnitude of the charging or discharging coefficient depends on the difference between the cylinder and set point pressures. A close examination of Figure 6b reveals that a Δp_c of about -0.9 psig is present for the charging process, while a 0.2 psig change is observed during the discharging phase. The discharging coefficient K_v is therefore likely to be different from the charging coefficient K_{sv}, since it corresponds to a significantly different operating region.

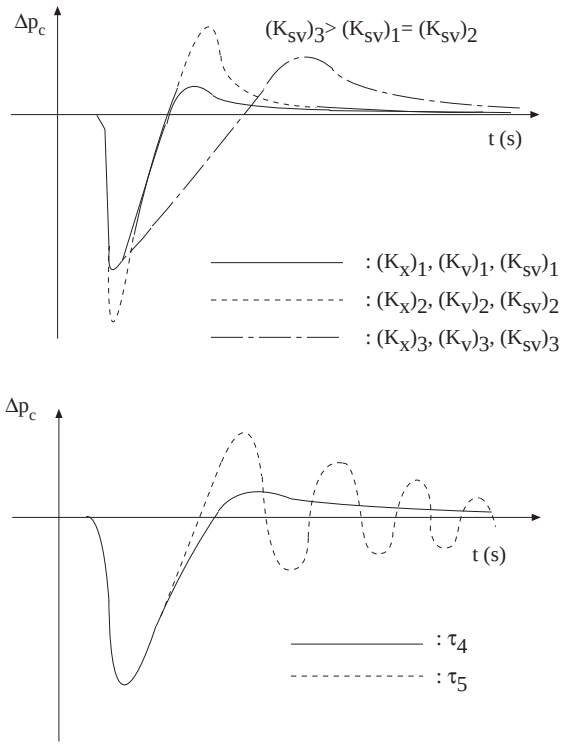

Figure 12. Effect of Pneumatic Model Parameters on Cylinder Pressure Response

The above argument is a good example of the effect of working at different operating regions of a nonlinear system. The model parameters for different operating regions are going to be significantly different. Moreover, the inherent nonlinear nature of the pneumatic system being examined rules out the use of linear superposition methods to determine the response to one piston displacement level using the known response for a different piston displacement level. Hence, the model parameters should be identified at piston displacement levels that will be experienced in practice.

A thinner gage block was used with the test setup in Figure 5, to give smaller displacements to the piston. Displacements of the order of 16 to 18 mils were found to be the lowest ones possible with the setup used. Step piston displacement tests were performed again by pulling the gage block off very quickly so that the piston moved a distance equal to the gage block thickness before hitting the mechanical stop. Experimental and simulated results are shown in Figures 13 and 14 for nominal pressures of 5 psig and 10 psig, respectively. The gage block could not be moved in a step fashion at higher nominal pressures. The model parameters obtained are listed in Table 2.

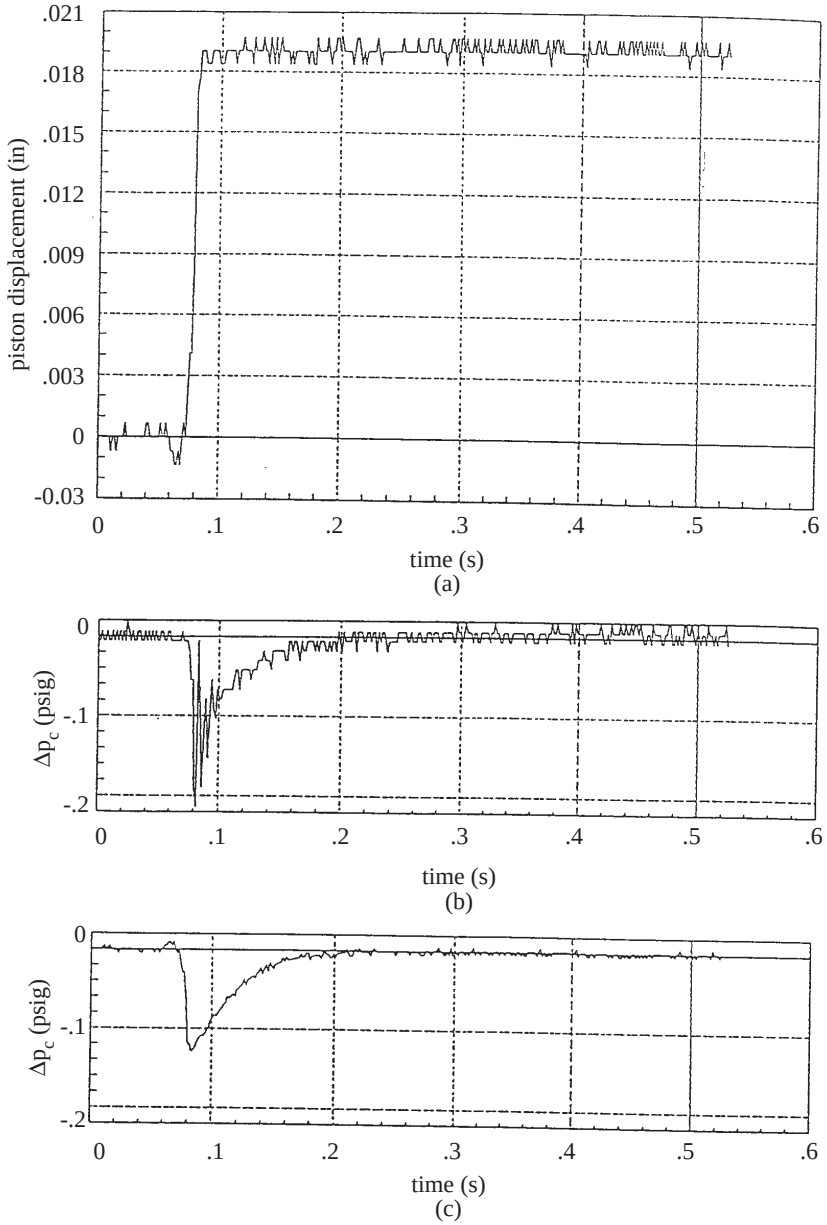

Figure 13. Cylinder Position Step Input Test for p_c=5 psig: a) Position Input. b) Change in Pressure. c) Simulated Change in Pressure

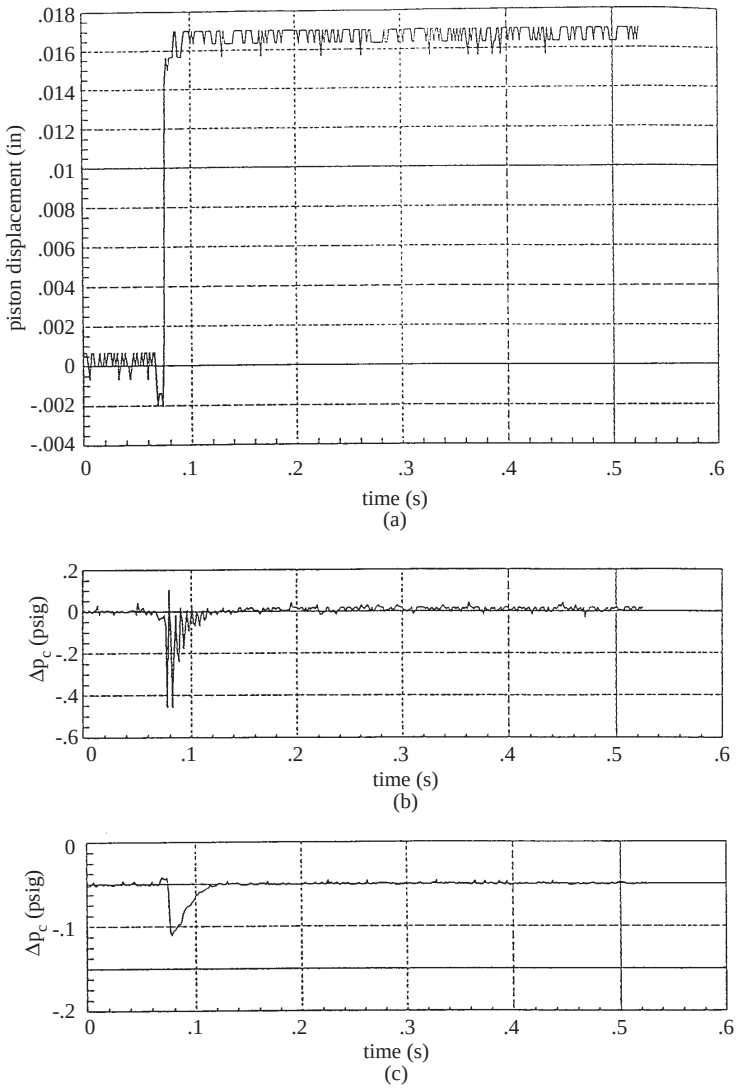

Figure 14. Cylinder Position Step Input Test for p_c=10 psig: a) Position Input. b) Change in Pressure. c) Simulated Change in Pressure

Table 2. Identified Pneumatic Model Parameters - Small Step

nominal pressure (psig)	K_x (lbf/in^3)	K_{sv} (s^{-1})	τ (s)
5	7.0	25.0	0.0075
10	15.7015	62.9682	0.0048

Note that the discharge coefficient K_v is not listed in Table 2. No discharging occurred during the smaller step tests (see Figures 13b and 14b), making it impossible to identify the value of K_v. There are also higher frequency oscillations present in these experimentally determined pressure responses. The possible reasons for this high frequency oscillatory behavior were explained above and their effect is more pronounced here since they are closer in magnitude to the smaller pressure changes observed now. The dynamic response of the pressure transducer's pressure sensing diaphragm is not expected to interfere with the measurements, since its mechanical resonance has been measured to be at approximately

450 Hz. The pressure fluctuations observed in Figures 13b and 14b are at about 200 Hz, lower than 450 Hz. It is reasonable to attenuate the higher frequency pressure changes by filtering since they are not of high practical interest here.

A comparison of the results in Tables 1 and 2 shows that all parameter values are smaller when smaller step displacements are used. This change in parameters is a consequence of the pneumatic system nonlinearities making the quasi-linearized model in Figure 4 dependent on the operating region. It is clear that the pneumatic model parameters should be identified for displacement levels consistent with those the pistons will be subjected to during actual operation of the device under study.

4. Discussion and Conclusions

In this paper, a pneumatic cylinder-pressure regulator combination is analyzed using lumped parameter modeling and small signal linearization. The pneumatic model obtained is nonlinear because of differences between the charging and discharging coefficients. This model is used to determine numerical values of model parameters for the regulator-cylinder used in a commercially available pneumatic constant force device. Step-like piston displacement tests are used to verify the repeatability of measured cylinder pressure changes when the nominal pressure was kept constant. Model parameter values are identified using maximum likelihood estimation. These model parameters resulted in close agreement between simulated and experimental cylinder pressures.

The effect of changes in model parameter values on pressure regulation is seen through experiments and simulation. The sensing chamber time constant does not affect pressure response if it is lower than 0.01 s. The charging and discharging coefficients affect the settling time of the response. The velocity input gain K_x, on the other hand, affects the peak in the cylinder pressure change. Experiments at different displacement levels result in significantly different numerical model parameter values. Hence, numerical values should be determined using input displacements that are characteristic of the application. If a range of displacements is anticipated, sets of pneumatic model parameters, each determined at one intermediate displacement level, should be used in subsequent analysis. Note that the method used here for modeling and numerical model parameter determination are general in nature and can be used in modeling of other devices with pneumatic regulator-cylinder pairs after small modifications.

Nomenclature

A	Cross-sectional area of the aspirator tube
A_{sv}	Effective supply to orifice area
A_v	Effective outlet to vent orifice area
D	Aspirator tube inner diameter
dM_a/dt	Mass flow rate through aspirator tube
dM_c/dt	Mass flow rate during charging
dM_d/dt	Mass flow rate during discharging
K	Charging or discharging gain
K_{sv}	Charging gain (s^{-1})
K_v	Discharging gain(s^{-1})
K_x	Velocity input gain(lbf/in^3)
K_1	Control chamber gain
K_2	Charging gain
K_3	Discharging gain
K_4	Supply valve gain
K_5	Relief valve gain
L	Aspirator tube length
M_a	Mass of air inside control chamber
n	Polytropic gas constant
p	Outlet pressure (psi)
p_c	Cylinder pressure (psi)
Δp_c	Change in cylinder pressure (psi)
p_d	Desired pressure (psi)
p_f	Control chamber pressure (psi)
p_s	Supply pressure (psi)
s	Laplace transform variable
T_s	Supply temperature
x_c	Piston position (in)
μ	Viscosity
ρ_{av}	Average density
τ	Control chamber sensing time constant (s)

References

Alvite, J. G., and Gearman, T. A., "Four New Constant Force Devices", Technical Paper, Mecanotron Corporation, Roseville, Minnesota, 1988.

Andersen, B. W., The Analysis and Design of Pneumatic Systems, Robert E. Krieger Publishing Company, Malabar, Florida, 1976.

Brevick, J. R., and Hanrath, G., "Automated Die and Mold Finishing: An Experimental Study of Short Stroke Honing", Proceedings of the 20^{th} North American Manufacturing Research Conference, 1992.

Güvenç, L., "Robot Assisted Polishing Using Non-programmable Active End Effectors", International Conference on Recent Advances in Mechatronics, (ed. Kaynak, O.), İstanbul, 100-105, 1999.

Güvenç, L., and Srinivasan, K., "Force Controller Design and Evaluation for Robot Assisted Die and Mold Polishing", Mechanical Systems and Signal Processing, 1, 31-49, 1995.

Graf, T. L., "Deburring and Finishing Applications Using Robots and Computerized Automation", Technical Paper, 3M Corporation, St. Paul, Minnesota, 1988.

Weule, H., and Timmermann, S., "Automation of the Surface Finishing in the Manufacturing of Dies and Molds", Annals of the CIRP, 39/1, 299-303, 1990.